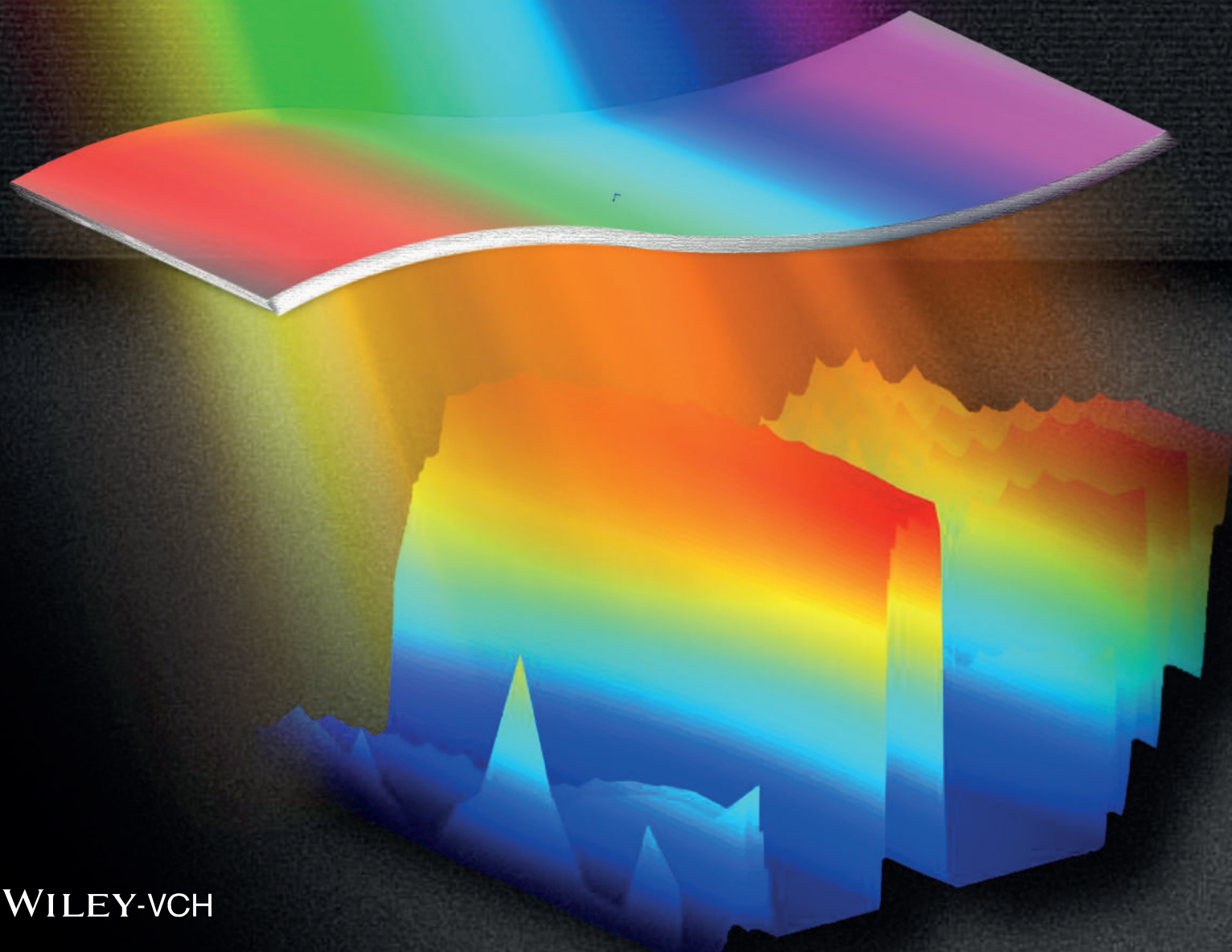


Vol. 6 • No. 15 • August 6 • 2018

www.advopticalmat.de

ADVANCED OPTICAL MATERIALS



WILEY-VCH

Check
updates

High Performance, Biocompatible Dielectric Thin-Film Optical Filters Integrated with Flexible Substrates and Microscale Optoelectronic Devices

Changbo Liu, Qianyi Zhang, Dan Wang, Guanlei Zhao, Xue Cai, Lizhu Li, He Ding, Kaiyuan Zhang, Huachun Wang, Deying Kong, Lan Yin, Lei Liu, Guisheng Zou, Lingyun Zhao, and Xing Sheng*

Miniaturized, wearable, and implantable optoelectronic devices and systems provide incomparable opportunities for applications in biomedical fields. Optical filters with wavelength selective reflective/transmissive responses that can be integrated onto these biointegrated platforms are critically important for high performance operation. Here, high quality, dielectric thin-film optical filters on unconventional substrates via transfer printing are reported. Designed filters formed on flexible substrates exhibit highly spectral selective transmission and reflection, with the maximum optical density at stop band reaching 6. Additionally, freestanding filter membranes are combined with microscale optoelectronic devices, achieving enhanced emission intensity for light-emitting diodes and spectral sensitivity for photovoltaic detectors. Finally, their *in vitro* cytotoxicity is evaluated within cell culture, and *in vivo* biocompatibility is supported in living animals. The presented results offer viable routes to high performance optical components for advanced biointegrated optoelectronic systems.


1. Introduction

Advanced optoelectronic devices play an important role in biomedical fields like bioimaging,^[1] epidermal sensing,^[2–4] phototherapy,^[5] and laser surgery.^[6] More recently, researchers have

Dr. C. Liu, Q. Zhang, X. Cai, L. Li, Dr. H. Ding, K. Zhang,
H. Wang, Prof. X. Sheng
Department of Electronic Engineering
Beijing National Research Center for Information Science and
Technology
Tsinghua University
Beijing 100084, China
E-mail: xingsheng@tsinghua.edu.cn

Q. Zhang, D. Wang, K. Zhang, D. Kong, Prof. L. Yin, Prof. L. Zhao
School of Materials Science and Engineering
Tsinghua University
Beijing 100084, China

G. Zhao, Prof. L. Liu, Prof. G. Zou
Department of Mechanical Engineering
Tsinghua University
Beijing 100084, China

 The ORCID identification number(s) for the author(s) of this article can be found under <https://doi.org/10.1002/adom.201800146>.

DOI: 10.1002/adom.201800146

been investing considerable efforts in the exploitation of implantable optoelectronic devices and systems, which have capabilities to deliver and receive optical power and signals directly within the deep tissue. Remarkable examples include the development of microscale, injectable light-emitting diodes (LEDs), photodetectors, and waveguides in flexible, stretchable, and even biodegradable forms for neural stimulation, fluorescence sensing, and prosthesis.^[7–10] In such implantable optoelectronic systems, optical filters serve as one of the key components, which selectively transmit, reflect, or absorb light in particular wavelengths, enabling numerous applications in areas such as fluorescence imaging,^[11,12] marker-free microscopy,^[13,14] and biochemical sensing.^[15] Conventional optical filters (longpass, shortpass, bandpass, etc.) typically consist

of carefully designed multilayer dielectric or metallic structures, which exhibit excellent optical performance in terms of their high optical densities (O.D.s) in the stop bands (O.D. > 6, i.e., transmittance < 10^{−6}), high transmittance in the passing bands (>90%), and sharp cutoff from transmission to reflection.^[16,17] These filter structures are commonly formed on rigid substrates like glasses via vacuum deposition techniques (evaporation, sputter, etc.) at elevated substrate temperatures (up to 300 °C) to obtain thin-film materials with high quality and stability.^[16] Such thick and rigid substrates hinder the integration of these high quality filters with microscale devices in wearable or implantable formats. In addition, high temperature and the potential use of ion beam bombardment to assist the film deposition are incompatible with many inorganic- and organic-based devices as well as flexible, stretchable, and biocompatible substrates.^[18,19] Filter structures can also be directly fabricated onto flexible substrates or formed by incorporating dye molecules or pigments directly into organic polymer films.^[20–23] However, these demonstrated flexible filters exhibit optical performance inferior to their counterparts on rigid glass substrates. Therefore, it is highly crucial to explore approaches to realize high performance thin-film optical filters on flexible and biocompatible substrates, and further heterogeneously integrate them with microscale optoelectronic devices for desirable biointegration. The recently

developed transfer printing–based assembly approaches provide a powerful solution to integrate high performance, thin-film optoelectronic devices and structures (for example, LEDs, solar cells, lasers, metamaterials, etc.) onto various unconventional substrates.^[24–29] In this study, we present high performance, thin-film, dielectric-based optical filters on flexible substrates by the transfer process. Their optical properties are simulated and measured, with results comparable to the filters on original glass substrates. Furthermore, these freestanding filter membranes are combined with microscale optoelectronic devices including gallium nitride (GaN)-based LEDs and gallium arsenide (GaAs)-based photovoltaic (PV) detectors, demonstrating highly selective spectral reflection and transmission, as well as the feasibility of device integration. Finally, *in vitro* and *in vivo* studies illustrate the biocompatibility of the filters and their capabilities for potential use in implantable optoelectronic systems. These results offer simple and reliable routes to various types of flexible optical filters that are manufacturable, transferable, and biocompatible, and provide unprecedented opportunities for high performance biointegrated optoelectronic systems.

2. Fabrication and Characterizations

The process flow to fabricate thin-film, freestanding optical filters via transfer printing approaches is schematically shown

in **Figure 1a**. As an example, a bandpass filter that selectively reflects blue and green photons (420–560 nm) and transmits yellow and red photons (560–620 nm) at normal incidence is designed and fabricated in this study. The filter structure consists of a series of titanium dioxide (TiO₂) and silicon dioxide (SiO₂) films with a total thickness of about 8 μm. Such a filter has potential applications in detecting and imaging yellow and red fluorescence signals with high sensitivities by rejecting blue and green excitation sources.^[30,31] The first step in the fabrication flow is to deposit a sacrificial layer onto single crystalline silicon (Si) wafers. In our experiments, materials that can serve as sacrificial layers include copper (Cu), magnesium (Mg), and germanium oxide (GeO_x). Designed dielectric filters comprising multilayered TiO₂ and SiO₂ films are formed on the sacrificial layer using ion beam-assisted deposition (IBAD), with Si substrates heated up to 300 °C. **Figure 1b** illustrates optical images of the filter coatings generated on optical K9 glass as well as Si substrates with different sacrificial layers (Cu, Mg, and GeO_x). Visual inspection of these samples indicates smooth, mirror-like surfaces, rendering different colors on different substrates at various tilted angles. Subsequently, a flat stamp made of polydimethylsiloxane (PDMS) elastomer is attached to the surface of the filter, serving as a temporary holder during the etching process of the sacrificial layer. The sacrificial layer is selectively undercut by appropriate etchants (HCl, FeCl₃, and H₂O₂-based aqueous solutions for Mg, Cu, and GeO_x, respectively),

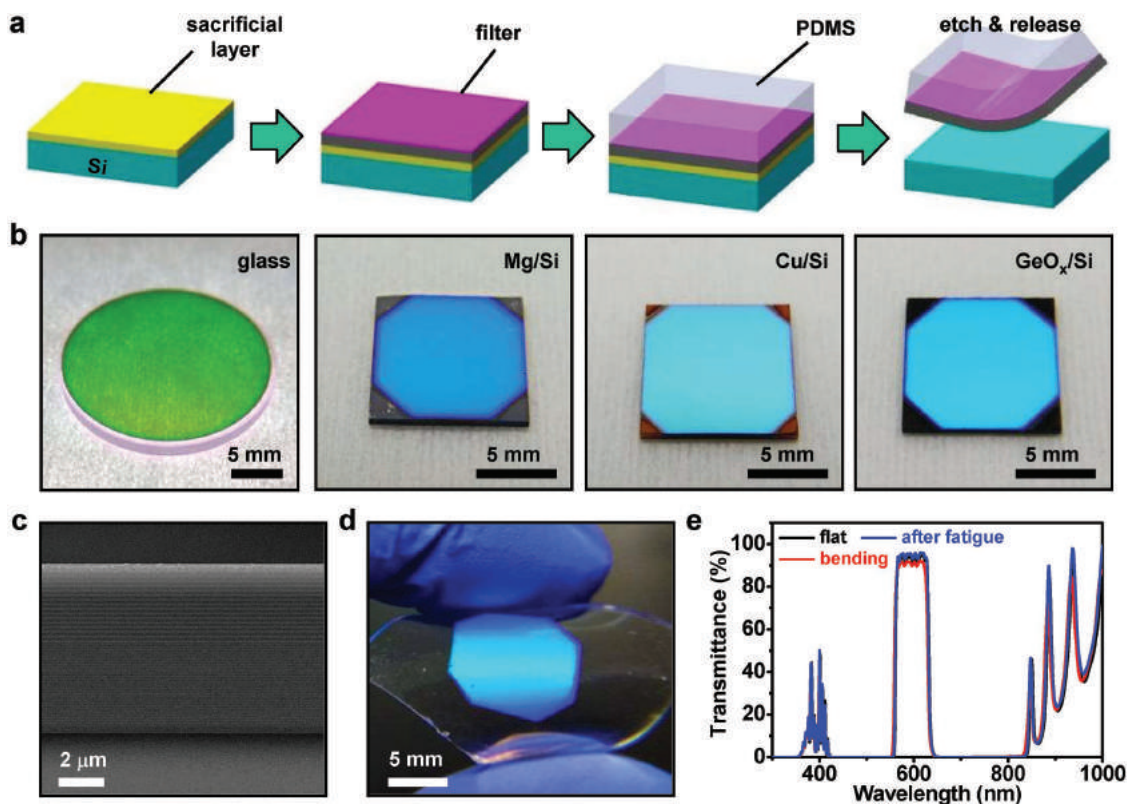


Figure 1. a) Schematic illustrations of the process flow to fabricate the flexible filter. b) Optical images (tilted view) of the filter layers deposited on glass and Si substrates with different sacrificial layers (Cu, Mg, and GeO_x). c) Scanning electron microscopic (SEM) image (cross-sectional view) of the filter structure, revealing multilayered periodic TiO₂/SiO₂ stacks. Bright and dark layers represent TiO₂ and SiO₂, respectively. d) Photograph of a released filter membrane on a flexible PDMS sheet. e) Transmission spectra of the flexible filter on PDMS: original flat (black), bending (red, bending radius 1 cm), after 200 times bending (blue).

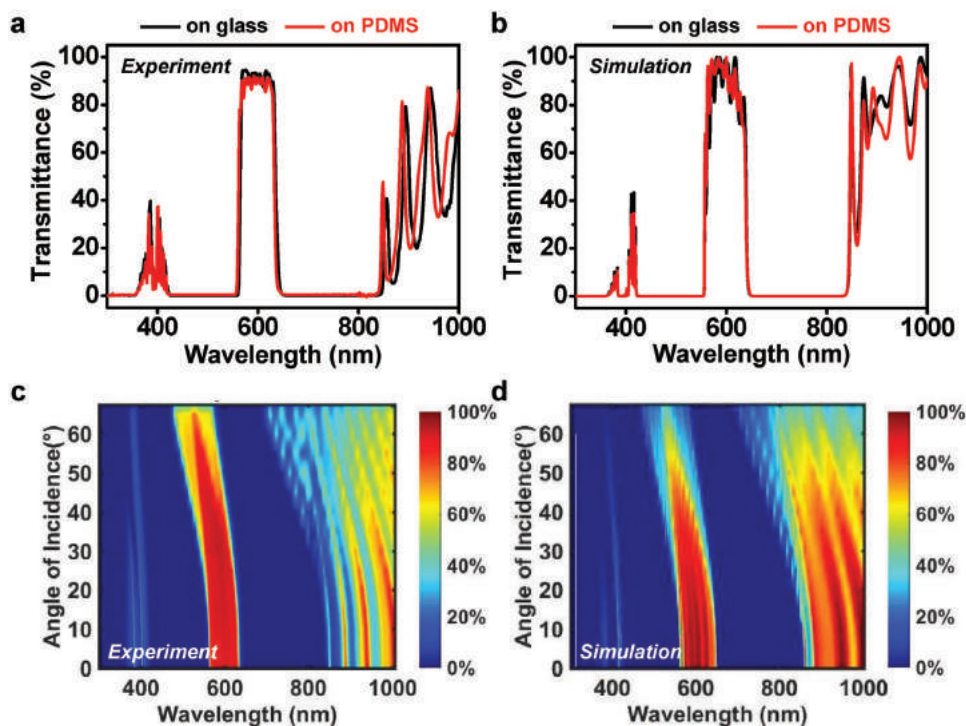


Figure 2. Optical performance of optical filters on glass and PDMS substrates. a) Measured and b) simulated transmission spectra for filters on glass and PDMS at normal incidence. c) Measured and d) simulated contour plots of angular-dependent transmission spectra for filters on PDMS.

releasing the thin-film filter structures from Si substrates. It is discovered that the releasing process carried out on Mg- and Cu-coated Si substrates renders high reproducibilities and success rates to form large area, freestanding membranes, while those filters on GeO_x sometimes form cracks and break into small pieces (see Figure S1 in the Supporting Information). The film quality is probably related to the residual stress during film deposition, and the details are worth further investigation. Corresponding scanning electron microscopic (SEM) cross-sectional image in Figure 1c illustrates the multilayered filter structure with periodic $\text{TiO}_2/\text{SiO}_2$ stacks that are optimized to obtain highly band selective transmission and reflection. A representative image of an intact freestanding thin-film filter (size $\approx 1 \text{ cm}^2$) released from Mg-coated Si onto a flexible PDMS sheet (bending radius $\approx 1 \text{ cm}$) is shown in Figure 1d. The filter membrane can be transferred onto target substrates in subsequent processes. Transmission spectra of flat and bended filters are presented in Figure 1e, demonstrating that their superior characteristics remain almost unaffected when bending. At a bending radius of $\approx 1 \text{ cm}$, the transmission slightly decreases in the transmission band and exhibits a small blueshift, which is attributed to the oblique incident angles on the curve surface. In addition, no crack or significant performance degradation is observed after the fatigue test under 200 cycles of bending. The filter's mechanical performance can be further improved by systematic structural designs (for example, embedding the film into the neutral plane^[32]) to mitigate the strain in the rigid dielectric layer. Such a transfer printing-based assembly approach provides unique opportunities to integrate these high performance filters with various heterogeneous materials and devices, when the direct deposition appears daunting due to the material

instability and expansion mismatch at elevated temperatures as well as the ion beam bombardment-induced damages.

Figure 2 plots measured and simulated performance of the filter on a flexible PDMS sheet, in comparison with the one on an original rigid glass substrate. At normal incidence, the filter exhibits a passing band between 560 and 620 nm, with transmittance $> 90\%$ (Figure 2a,b). Considering that K9 glass and PDMS have similar optical properties at visible wavelengths, similar results are obtained for filters on these substrates, revealing that the filter structure and performance are preserved during the transfer process. Furthermore, optical transmission in the stop band (420–550 nm) is measured to be less than 10^{-6} , reaching an O.D. of at least 6. By contrast, the O.D. of a commercially available flexible filter based on dyed sublayers of acrylate polymer is 2,^[33] and for a dye-doped PDMS-based flexible filter (total thickness $\approx 1 \text{ mm}$), its O.D. is 4.^[23] The optical characteristics of our flexible filters are also superior to other reported ones.^[20–22,32,34,35] Contour plots of measured and simulated transmission spectra at various incident angles for filters on PDMS are presented in Figure 2c,d, respectively. At oblique angles, the passing band shifts to shorter wavelengths due to the enhanced effective indices.^[17] Additionally, simulated transmission spectra are in agreement with experimental results (Figure 2b,d), indicating that the numerical tools provide capabilities to design and predict the filter performance very accurately.

3. Device Integration and Performance

These released thin-film filters are heterogeneously integrated with active optoelectronic devices to further explore their

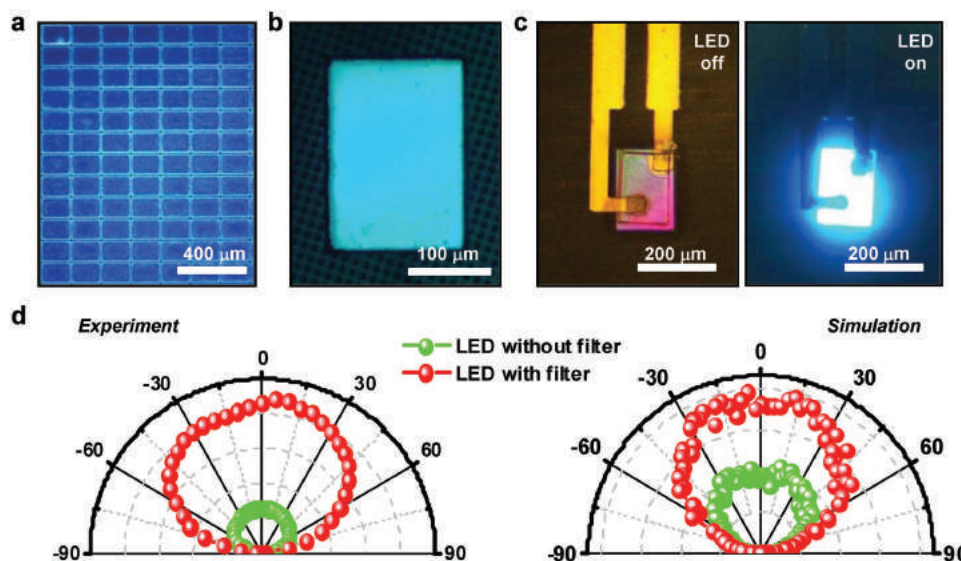


Figure 3. a) Optical image of filters diced by laser milling. b) Microscopic image of a patterned filter ($150\ \mu\text{m} \times 200\ \mu\text{m}$) mounted on the PDMS stamp. c) Images of the microscale blue GaN LED stacked on a filter structure, with LED turned on (right) and off (left). d) Measured (left) and simulated (right) angular emission profiles for micro-LEDs with and without filters in the bottom (in arbitrary units).

functionalities. The high O.D. in the stop band (420–550 nm) measured in Figure 2 indicates that the fabricated filter can achieve near-unity (>99%) reflectance in these wavelengths. Therefore, it can be utilized as a perfect mirror to improve the emission intensity of thin-film blue LEDs, as shown in Figure 3. The microscale GaN-based blue LEDs used here have an emission peak at 470 nm and a size of $125\ \mu\text{m} \times 180\ \mu\text{m}$, and the details of their fabrication process and performance are described in previous work.^[36] To match with the dimension of the LED, the filter illustrated in Figure 1b is first patterned into grid forms (size $\approx 150\ \mu\text{m} \times 200\ \mu\text{m}$) down to the sacrificial layer by laser milling, and then released by undercutting the sacrificial layer (Figure 3a). The released filters are individually picked up by PDMS stamps (Figure 3b) and transferred onto polyimide substrates. A microscale blue LED is further stacked onto the filter layer and metalized (Figure 3c). Far-field angular emission profiles of the micro-LEDs with and without the filter-based reflectors are measured and compared with ray tracing simulation results (Figure 3d). Lambertian radiation patterns are observed for both the devices, and the LED emission intensity in the front side is significantly enhanced at least by a factor of 2 using the filter in the backside, clearly demonstrating the highly reflective behavior (at 470 nm) of the band selective filter.

The thin-film filter is further integrated with microscale thin-film PV detectors to demonstrate its capability for band selective photodetection (Figure 4). GaAs-based detectors (size $\approx 700\ \mu\text{m} \times 700\ \mu\text{m}$, thickness $\approx 3.7\ \mu\text{m}$) are transferred onto glass substrates after epitaxial liftoff,^[37,38] with the released filter membrane printed on the device surface after encapsulation and metallization. The images of detectors with and without filters are shown in Figure 4a. External quantum efficiency (EQE) spectra of both the GaAs detectors are measured and simulated, presented in Figure 4b–d. As shown in Figure 4b, a bare GaAs detector exhibits broadband spectral sensitivities, covering the entire visible and part of the near-infrared ranges (400–900 nm). It is noted that no antireflective coatings (ARCs)

are implemented on these GaAs detectors, and the spectral response of these detectors can be further improved from about 60% to more than 90% by optimizing ARCs^[25] in the future. By employing the designed thin-film filter on the device surface, the spectral sensitive region is limited to 560–620 nm in the visible range at normal incidence (Figure 4c,d), demonstrating high spectrum selectivity. At larger incident angles, EQE spectra shift to shorter wavelengths, in agreement with the filter properties presented in Figure 2. Such microscale detectors integrated with designer filters show promises for detecting fluorescence of chemical species and biomarkers in selective bands.^[39,40]

4. Biocompatibility Evaluation

The unique features and properties of such a flexible and miniaturized thin-film filter can potentially serve as a vital component in wearable and implantable optoelectronic systems. It is critically necessary to evaluate its biocompatibilities. One of the key aspects is to assess its cytotoxicity. L929 mouse fibroblast cell lines are cultured on filters, and the cell behavior is analyzed by fluorescence imaging after 1, 3, and 7 days. As presented in Figure 5a, living and dead cells are marked with green and red fluorescence, respectively. L929 fibroblasts interact and adhere to the samples, proliferating significantly within 7 days. Cells cultured on both bare glass (negative control) and filter-coated glasses maintain their characteristic morphologies. Regarding to their number and distribution, there is no significant difference between these two groups. Figure 5b summarizes the viability of cells determined by a live/dead cell count from three different areas on each sample. The viability is high for both the types of samples during the incubation, displaying no signs of cytotoxicity.

Figure 5c,d further investigates *in vivo* biocompatibilities of these released thin-film filters, by implanting them subcutaneously in back and skull regions of the healthy male Sprague

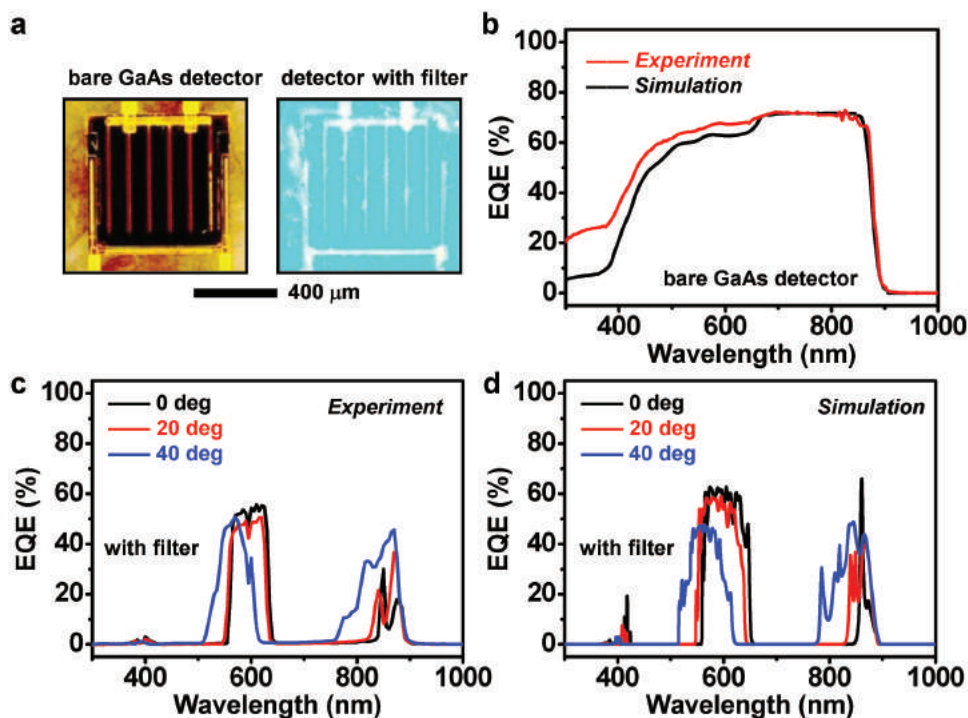


Figure 4. Performance of GaAs-based photodetectors integrated with freestanding filters. a) Images of GaAs detectors with (left) and without (right) the filter. b) Measured and simulated EQE spectra of the bare GaAs detector. c) Measured and d) simulated EQE spectra of the GaAs detector with the filter at different incident angles.

Dawley (SD) rats. The evaluations of the tissues adjacent to the filters are conducted after 1, 2, and 5 weeks, respectively. From the captured images of the skin in Figure 5c, macroscopic evaluation of the implantation site shows that the filter adheres to a transparent layer of connective tissues, and no obvious signs of pathological inflammatory tissue responses to the filter implantation are observed. Tissues covering the filters are retrieved and stained with hematoxylin and eosin (H&E). The histological analyses of the tissues show the accumulation of neutrophils and macrophages around the implants during the first 2 weeks (Figure 5d). Considering their number and distribution, the overall inflammatory are graded minimal,^[41] indicating ideal biocompatibility of the implants. Meanwhile, there is an appreciable increase of fibroblasts and a sprout of capillaries, marking the commencement of proliferative phase. Thick collagen fibers are observed around the implants. The left and the right images, which are from surrounding tissues (≈ 2 mm away), show no sign of infection and inflammation, indicating that the influence of the implant is within a small area. On the whole, the wound closure is clean without tissue loss and the healing process is smooth and prompt, therefore the process belongs to healing by primary intention.^[42] The desirable biocompatibility of these implantable filters can be attributed to the high stability of the TiO_2 and SiO_2 base dielectric materials that are used to form the filter structure.^[10,43]

5. Conclusion

In conclusion, we present high performance, dielectric-based flexible thin-film filters based on transfer printing methods.

These flexible filters obtained in this study not only illustrate their utilities to modulate device performance when integrating with microscale LEDs and PV detectors, but also exhibit ideal biocompatibilities both in vitro and in vivo. As an essential optical component, such filters can be readily implemented into wearable and implantable optoelectronic systems for biomedical uses, including fluorescence sensing, optogenetic interrogation, and health monitoring.^[4,44,45] Besides LEDs and photodetectors, such filters can also be combined with other photonic devices such as microscale lasers and waveguides for versatile applications like beam steering and spectral shaping.^[32,46] Other research efforts would include the use of phase change materials to offer additional features like tunable and reconfigurable optical behaviors.^[47,48] In bioresorbable device systems for potential clinical uses,^[49,50] it is envisioned that biodegradable materials (like SiO_2 , MgO , Si, polymers, etc.) can be incorporated to realize natural degradation after implantation. To summarize, these findings clear away obstacles in universal fabrication of high performance flexible filters and open the door for their broad applications in biointegrated optoelectronic systems.

6. Experimental Section

Filter Design and Optimization: The transfer-matrix method^[17] was employed to design the filter structure (details are provided in the Supporting Information), which comprised alternating layers of high-refractive-index titanium dioxide (TiO_2) and low-refractive-index silicon dioxide (SiO_2) with their optical properties extracted from the literature.^[51] In the initial design, the multilayer filter consisted of two

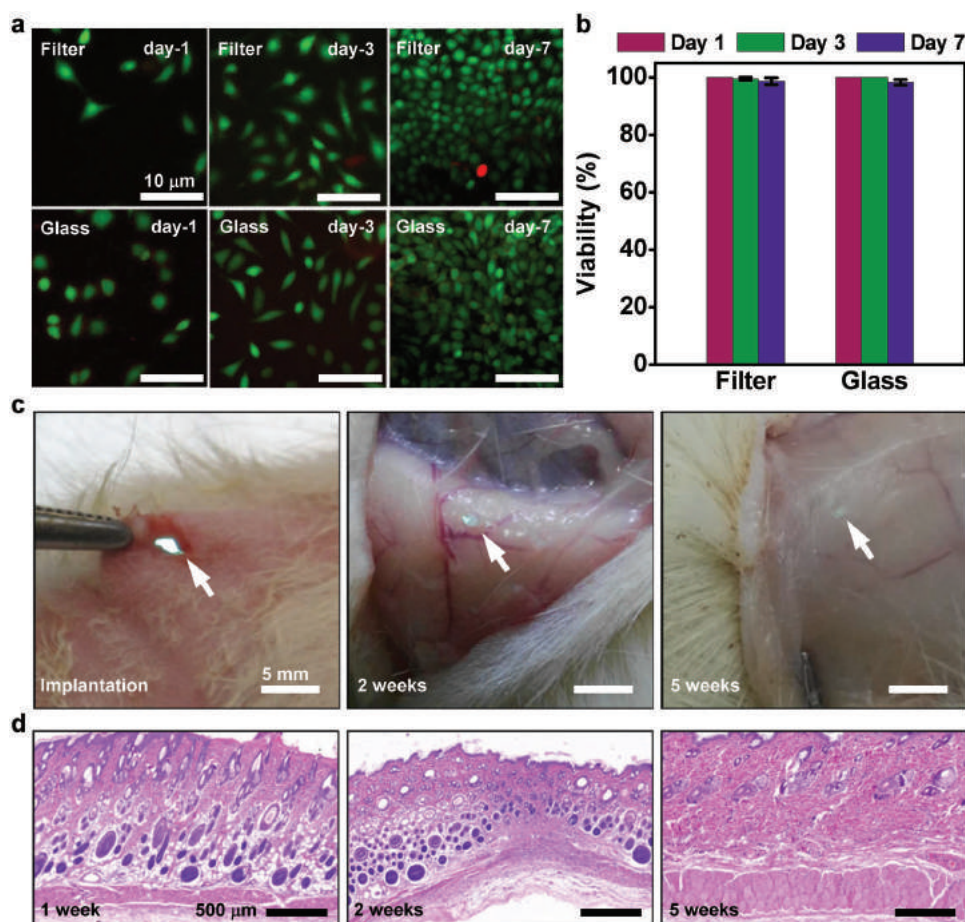


Figure 5. In vitro and in vivo biocompatibility tests of the released flexible filter. a) Fluorescent images showing the proliferation behavior for L929 cell lines cultured on glasses with and without filter coatings. Green and red fluorescence represent live and dead cells (L929 fibroblasts), respectively. b) Comparison of cell viability on glasses with and without filter coatings over 1, 3, and 7 days, with results calculated as the fraction of total cells. c) Optical images of implantation process (left) and filters being retrieved after 2 and 5 weeks of subcutaneous implantation in Sprague-Dawley rats. Arrows indicating the filters embedded in tissue. d) Histological evaluation of the effect of subcutaneous implants on surrounding tissue (stained with H&E) after 1, 2, and 5 weeks of implantation. Healing by primary intention.

periodic substructures and each substructure was a stack of alternate TiO_2 and SiO_2 films. One substructure had 17 periods of 86 nm TiO_2 and 120 nm SiO_2 , and the other had 32 periods of 53 nm TiO_2 and 78 nm SiO_2 . A freely available software package (OpenFilters)^[52] was used to calculate and optimize the filter performance. The optimized filter had a structure of 146 nm TiO_2 /26 nm SiO_2 /81 nm TiO_2 /104 nm SiO_2 /107 nm TiO_2 /17 periods of 120 nm SiO_2 + 86 nm TiO_2 /18 nm SiO_2 /38 nm TiO_2 /32 periods of 78 nm SiO_2 + 53 nm TiO_2 /64 nm SiO_2 /35 nm TiO_2 , with a total thickness of 8.3 μm .

Fabrication of Flexible Optical Filters: Silicon (Si) {100} wafers served as the substrates for forming the multilayered dielectric optical filters. Materials used as sacrificial layers included Cu, Mg, and GeO_x . Cu, Mg, and Ge thin films were, respectively, deposited on the Si substrates by sputtering, and the thicknesses of all these films were 500 nm. GeO_x films were formed by thermally oxidizing the deposited Ge film at 500 °C for 5 h in air (with a heating rate of 8 °C min^{-1} , self-cooling to room temperature afterward). The designer TiO_2 / SiO_2 filter structure was subsequently coated onto the Si wafers with sacrificial layers as well as bare K9 glasses using ion beam-assisted sputter deposition, with substrates heated up to 300 °C (HB-Optical, Shenyang, China). Different etchants were utilized to selectively remove the different sacrificial layers between the filter and Si. The corresponding etchants were FeCl_3 solution (FeCl_3 : H_2O = 1:1 weight ratio) for Cu (etch rate \approx 0.3 mm h^{-1}), diluted HCl (HCl : H_2O = 1:1 volume ratio) for Mg (etch rate \approx 2 mm h^{-1}),

and diluted H_2O_2 (H_2O_2 : H_2O = 1:1) for GeO_x (etch rate \approx 0.05 mm h^{-1}). It was discovered that the Mg layer rendered the optimal undercut results with minimum defects formed in the freestanding filter layer after etching. Released, freestanding filters could be picked up by PDMS stamps (Dow Corning Sylgard 184 kit, 1:10 weight ratio) and transferred onto any substrates. Laser milling (Nd:YVO₄ laser, 1064 nm) was applied to form the filters with designed patterns and shapes.

Integration of Filters with LEDs and Detectors: Freestanding, laser-patterned filters were transferred onto polyimide with a thin-film polymer as an adhesive. The thin-film microscale blue LED structure (from bottom to top) consisted of a GaN buffer layer, a n-GaN layer, an InGaN/GaN multiple-quantum-well layer, and a p-GaN layer, with a total thickness of about 7.1 μm . The GaN-based micro-LEDs were grown on flat sapphire substrates and released after laser liftoff.^[39] The thin-film, microscale GaAs-based PV detector structure (from bottom to top) included a p-GaAs contact layer, an $\text{Al}_{0.3}\text{Ga}_{0.7}\text{As}$ back surface field (BSF), a p-GaAs base layer, a n-GaAs emitter layer, and an InGaP window layer, with a total thickness of about 3.7 μm . The GaAs detectors were grown on GaAs substrates and released after etching the AlAs-based sacrificial layer.^[38] These fabricated microscale devices were transferred onto flexible polyimide substrates by PDMS stamps, with patterned filters integrated on the bottom of the GaN LEDs and on the top of the GaAs detectors, respectively. A 2 μm thick SU-8 film was used as the adhesion layer. The interconnected metal electrodes that consisted of 20 nm Cr/500 nm Cu/100 nm Au were formed by sputtering.

Device Characterization: The SEM image was captured by ZEISS Merlin microscope (15 kV). The optical microscopy images were taken by microscope MC-D800U(C). The transmittance spectra of the optical filters were measured using a UV-vis-IR spectrophotometer (Cary 5000, Varian). Typical scans were performed from 300 to 1000 nm with a 2 nm resolution at every 5° from 0° to 70°, and the incident probe beam spot had a diameter of 1 mm. The O.D. at the filter stop band was measured at 470 nm using a laser source (MBL-FN-473 Solid State), calibrated by a standard Si photodetector (DET36A, Thorlabs). At specific wavelengths, O.D. is defined as $\log_{10}(I_0/I_{\text{transmission}})$, where I_0 and $I_{\text{transmission}}$ respectively, refer to the incident light power and transmitted light power after passing the filter. The LEDs were mounted onto a goniometer for angular emission intensity measurement from -90° to 90° in steps of 5°, at an injection current of 3 mA. The emission intensity was captured by a standard Si photodetector (DET36A, Thorlabs). The EQE spectra of the GaAs detector (incidence from 0° to 40°) were measured using a quantum efficiency measurement system (QEX10) from 300 to 1000 nm with a 5 nm resolution.

Device Simulation: The emission profiles of the stacked LED/filter structures were modeled by using Monte Carlo-based ray tracing methods (TracePro free trial version).^[53] The file source emitted light with the wavelength of 470 nm toward all directions obeying Lambert's cosine law. All surfaces of structures in the model were considered as smooth planes without surface scattering. The simulated EQE spectra for detectors with and without filters on top were obtained based on the transfer-matrix method^[7] (see the Supporting Information for details) using OpenFilters.^[52]

In Vitro Cytotoxicity Study: Glass substrates with and without the designed optical filter coating were sterilized in 70% ethanol followed by ultraviolet (UV) irradiation for 3 days. L929 fibroblastic cells (ATCC, USA) were cultured in the Roswell Park Memorial Institute (RPMI)-1640 (Gibco Life Technologies, China) medium with 10% fetal bovine serum (FBS) and 1% penicillin-streptomycin in a humid atmosphere containing 5% CO₂. The cell culture medium was replaced every day. Cells were then seeded on samples at a density of 300 cells mm⁻². Live/dead staining was conducted after the cells were incubated for 1, 3, and 7 days to qualitatively evaluate the cell viability. Calcein-AM and propidium iodide (Gibco Life Technologies, China) were used to stain live and dead cells, respectively. Before the analysis of cell proliferation, the cell-laden constructs were washed with phosphate buffered saline (PBS) twice and stained with Calcein-AM and propidium iodide for 20 min. A confocal microscope (Leica, Germany) was used to determine the distribution of living and dead cells on the samples. The numbers of live and dead cells in three randomly selected fields were counted and values were calculated based on the average percentage of living cells based on total cells to measure the viability of cells.^[54]

In Vivo Biocompatibility Study: Filter samples used in the in vivo experiment were dipped in 70% ethanol and exposed to UV radiation so as to minimize the risk of infection. Healthy male SD rats (Beijing Vital River Laboratory Animal Technology, China) of 4 weeks were employed in this study to evaluate the biocompatibility of the flexible filters. The skin region of surgery was shaved and prepared aseptically for operation and the animals were anesthetized by gas concentration of 2.5% isoflurane during the process. After the standard transversal incision of 3–5 mm was made, a piece of flexible filter (diameter: ≈2.0 mm) was placed in subcutaneous space. The blank control group was operated as the control group but placed nothing. Then, the wound was closed by suturing. The whole process was under sterile conditions and the rats were held in standard conditions both prior to and after implantation. The in vivo biocompatibility of flexible filters was evaluated after embedding filters under the back and skull skin of SD rats. At 1, 2, and 5 weeks after implantation, rats were euthanized in carbon dioxide chamber. Photographs of pieces of filter in subcutaneous tissues were taken. Then, the implants and the surrounding tissues were carefully collected from the body. Samples were soaked in formalin for 3 days in order to fix the tissue. Then, they went through biopsy process and were stained with H&E for histological examination. The slices were photographed with optical microscope (Nikon, Eclipse CI). Animal

care is in accordance with the institutional guidelines of the Tsinghua University. Protocols are proved by the Institutional Animal Care and Use Committee (IACUC) in the Tsinghua University.

Supporting Information

Supporting Information is available from the Wiley Online Library or from the author.

Acknowledgements

C.L. and Q.Z. contributed equally to this work. L.Y. and X.S. acknowledge the support from the National Natural Science Foundation of China (NSFC Projects 51602172 and 51601103) and the 1000 Youth Talents Program in China. X.S. also acknowledges support from the Science and Technology Innovation Commission of Shenzhen (JCYJ20170411140807570).

Conflict of Interest

The authors declare no conflict of interest.

Keywords

flexible photonics, implantable devices, optical filters, optoelectronics

Received: February 4, 2018

Revised: April 3, 2018

Published online: May 16, 2018

- [1] D. Arndt-Jovin, M. Robert-Nicoud, S. Kaufman, T. Jovin, *Science* **1985**, 230, 247.
- [2] D.-H. Kim, N. Lu, R. Ma, Y.-S. Kim, R.-H. Kim, S. Wang, J. Wu, S. M. Won, H. Tao, A. Islam, K. J. Yu, T.-i. Kim, R. Chowdhury, M. Ying, L. Xu, M. Li, H.-J. Chung, H. Keum, M. McCormick, P. Liu, Y.-W. Zhang, F. G. Omenetto, Y. Huang, T. Coleman, J. A. Rogers, *Science* **2011**, 333, 838.
- [3] T. Yokota, P. Zalar, M. Kaltenbrunner, H. Jinno, N. Matsuhsa, H. Kitanosako, Y. Tachibana, W. Yukita, M. Koizumi, T. Someya, *Sci. Adv.* **2016**, 2, 8.
- [4] H. Araki, J. Kim, S. Zhang, A. Banks, K. E. Crawford, X. Sheng, P. Gutruf, Y. Shi, R. M. Pielak, J. A. Rogers, *Adv. Funct. Mater.* **2017**, 27, 1604465.
- [5] V. P. Zharov, Y. A. Menyayev, V. A. Hamaev, G. M. Antropov, M. Waner, presented at BiOS 2000, The Int. Symp. on Biomedical Optics, San Jose, CA, January **2000**.
- [6] E. Young, A. Mitchell-Innes, M. Jindal, *J. Laryngol. Otol.* **2015**, 129, 627.
- [7] R. Fu, W. Luo, R. Nazempour, D. Tan, H. Ding, K. Zhang, L. Yin, J. Guan, X. Sheng, *Adv. Opt. Mater.* **2018**, 6, 1700941.
- [8] T. I. Kim, J. G. McCall, Y. H. Jung, X. Huang, E. R. Siuda, Y. Li, J. Song, Y. M. Song, H. A. Pao, R. H. Kim, C. Lu, S. D. Lee, I. S. Song, G. Shin, R. Al-Hasani, S. Kim, M. P. Tan, Y. Huang, F. G. Omenetto, J. A. Rogers, M. R. Bruchas, *Science* **2013**, 340, 211.
- [9] Y. M. Song, Y. Xie, V. Malyarchuk, J. Xiao, I. Jung, K. J. Choi, Z. Liu, H. Park, C. Lu, R. H. Kim, R. Li, K. B. Crozier, Y. Huang, J. A. Rogers, *Nature* **2013**, 497, 95.

- [10] K. Mathieson, J. Loudin, G. Goetz, P. Huie, L. Wang, T. I. Kamins, L. Galambos, R. Smith, J. S. Harris, A. Sher, D. Palanker, *Nat. Photonics* **2012**, *6*, 391.
- [11] A. Corlu, R. Choe, T. Durduran, M. A. Rosen, M. Schweiger, S. R. Arridge, M. D. Schnall, A. G. Yodh, *Opt. Express* **2007**, *15*, 6696.
- [12] Q. Wei, H. Qi, W. Luo, D. Tseng, S. J. Ki, Z. Wan, Z. Göröcs, L. A. Bentolila, T.-T. Wu, R. Sun, A. Ozcan, *ACS Nano* **2013**, *7*, 9147.
- [13] Y. Cotte, F. Toy, P. Jourdain, N. Pavillon, D. Boss, P. Magistretti, P. Marquet, C. Depeursinge, *Nat. Photonics* **2013**, *7*, 113.
- [14] K. Lee, K. Kim, J. Jung, J. Heo, S. Cho, S. Lee, G. Chang, Y. Jo, H. Park, Y. Park, *Sensors* **2013**, *13*, 4170.
- [15] T. A. Guo, F. Liu, B. O. Guan, J. Albert, *Opt. Laser Technol.* **2016**, *78*, 19.
- [16] C. Madsen, J. H. Zhao, *Optical Filter Design and Analysis: A Signal Processing Approach*, Wiley, New York, USA **1999**.
- [17] H. A. Macleod, *Thin-Film Optical Filters*, IOP Publishing, Bristol, UK **2001**.
- [18] W. Ensinger, *Nucl. Instrum. Methods Phys. Res., Sect. B* **1995**, *106*, 142.
- [19] K. G. Ressler, N. Sonnenberg, M. J. Cima, *J. Am. Ceram. Soc.* **1997**, *80*, 2637.
- [20] W. Zhou, Z. Ma, H. Yang, Z. Qiang, G. Qin, H. Pang, L. Chen, W. Yang, S. Chuwongin, D. Zhao, *J. Phys. D: Appl. Phys.* **2009**, *42*, 234007.
- [21] P. Reader-Harris, A. Ricciardi, T. Krauss, A. Di Falco, *Opt. Express* **2013**, *21*, 1002.
- [22] A. D. Falco, Y. Zhao, A. Alú, *Appl. Phys. Lett.* **2011**, *99*, 163110.
- [23] O. Hofmann, X. Wang, A. Cornwell, S. Beecher, A. Raja, D. D. C. Bradley, A. J. deMello, J. C. deMello, *Lab Chip* **2006**, *6*, 981.
- [24] D. Chanda, K. Shigeta, S. Gupta, T. Cain, A. Carlson, A. Mihi, A. J. Baca, G. R. Bogart, P. Braun, J. A. Rogers, *Nat. Nanotechnol.* **2011**, *6*, 402.
- [25] X. Sheng, C. A. Bower, S. Bonafede, J. W. Wilson, B. Fisher, M. Meitl, H. Yuen, S. Wang, L. Shen, A. R. Banks, C. J. Corcoran, R. G. Nuzzo, S. Burroughs, J. A. Rogers, *Nat. Mater.* **2014**, *13*, 593.
- [26] X. Sheng, C. Robert, S. Wang, G. Pakeltis, B. Corbett, J. A. Rogers, *Laser Photonics Rev.* **2015**, *9*, L17.
- [27] M. A. Meitl, Z.-T. Zhu, V. Kumar, K. J. Lee, X. Feng, Y. Y. Huang, I. Adesida, R. G. Nuzzo, J. A. Rogers, *Nat. Mater.* **2005**, *5*, 33.
- [28] A. Carlson, A. M. Bowen, Y. Huang, R. G. Nuzzo, J. A. Rogers, *Adv. Mater.* **2012**, *24*, 5284.
- [29] S. I. Park, Y. Xiong, R. H. Kim, P. Elvikis, M. Meitl, D. H. Kim, J. Wu, J. Yoon, C. J. Yu, Z. Liu, Y. Huang, K. C. Hwang, P. Ferreira, X. Li, K. Choquette, J. A. Rogers, *Science* **2009**, *325*, 977.
- [30] N. C. Shaner, R. E. Campbell, P. A. Steinbach, B. N. G. Giepmans, A. E. Palmer, R. Y. Tsien, *Nat. Biotechnol.* **2004**, *22*, 1567.
- [31] E. M. Merzlyak, J. Goedhart, D. Shcherbo, M. E. Bulina, A. S. Shcheglov, A. F. Fradkov, A. Gaintzeva, K. A. Lukyanov, S. Lukyanov, T. W. J. Gadella, D. M. Chudakov, *Nat. Methods* **2007**, *4*, 555.
- [32] Y. Zou, D. Zhang, H. Lin, L. Li, L. Moreel, J. Zhou, Q. Du, O. Ogbuu, S. Danto, J. D. Musgraves, K. Richardson, K. D. Dobson, R. Birkmire, J. Hu, *Adv. Opt. Mater.* **2014**, *2*, 478.
- [33] Edmund, Ultra-Thin Longpass Filters, <https://www.edmundoptics.com/resources/trending-in-optics/ultra-thin-longpass-filter/> (accessed: January 2018).
- [34] L. Xu, Y. Yao, N. D. Bronstein, L. Li, A. P. Alivisatos, R. G. Nuzzo, *ACS Photonics* **2016**, *3*, 278.
- [35] H. Ning, N. A. Krueger, X. Sheng, H. Keum, C. Zhang, K. D. Choquette, X. Li, S. Kim, J. A. Rogers, P. V. Braun, *ACS Photonics* **2014**, *1*, 1144.
- [36] L. Li, C. Liu, Y. Su, J. Bai, J. Wu, Y. Han, Y. Hou, S. Qi, Y. Zhao, H. Ding, Y. Yan, L. Yin, P. Wang, Y. Luo, X. Sheng, *Adv. Mater. Technol.* **2018**, *3*, 1700239.
- [37] X. Sheng, L. Shen, T. Kim, L. Li, X. Wang, R. Dowdy, P. Froeter, K. Shigeta, X. Li, R. G. Nuzzo, N. C. Giebink, J. A. Rogers, *Adv. Energy Mater.* **2013**, *3*, 991.
- [38] X. Sheng, M. H. Yun, C. Zhang, A. a. M. Al-Okaily, M. Masouraki, L. Shen, S. Wang, W. L. Wilson, J. Y. Kim, P. Ferreira, X. Li, E. Yablonovitch, J. A. Rogers, *Adv. Energy Mater.* **2015**, *5*, 1400919.
- [39] A. Gomes, E. Fernandes, J. L. F. C. Lima, *J. Biochem. Biophys. Methods* **2005**, *65*, 45.
- [40] A. B. Chinen, C. M. Guan, J. R. Ferrer, S. N. Barnaby, T. J. Merkel, C. A. Mirkin, *Chem. Rev.* **2015**, *115*, 10530.
- [41] T. M. Macleod, G. Williams, R. Sanders, C. J. Green, *Br. J. Plast. Surg.* **2005**, *58*, 518.
- [42] V. Kumar, A. K. Abbas, J. C. Aster, *Robbins Basic Pathology*, Elsevier, Philadelphia, PA, USA **2017**.
- [43] Y. Wang, C. Wen, P. Hodgson, Y. Li, *J. Biomed. Mater. Res., Part A* **2014**, *102*, 743.
- [44] G. Shin, A. M. Gomez, R. Al-Hasani, Y. R. Jeong, J. Kim, Z. Xie, A. Banks, S. M. Lee, S. Y. Han, C. J. Yoo, J. L. Lee, S. H. Lee, J. Kurniawan, J. Tureb, Z. Guo, J. Yoon, S. I. Park, S. Y. Bang, Y. Nam, M. C. Walicki, V. K. Samineni, A. D. Mickle, K. Lee, S. Y. Heo, J. G. McCall, T. Pan, L. Wang, X. Feng, T. I. Kim, J. K. Kim, Y. Li, Y. Huang, R. W. Gereau, J. S. Ha, M. R. Bruchas, J. A. Rogers, *Neuroendocrinology* **2017**, *93*, 509.
- [45] L. Lu, P. Gutruf, L. Xia, D. L. Bhatti, X. Wang, A. Vazquez-Guardado, X. Ning, X. Shen, T. Sang, R. Ma, G. Pakeltis, G. Sobczak, H. Zhang, D.-o. Seo, M. Xue, L. Yin, D. Chanda, X. Sheng, M. R. Bruchas, J. A. Rogers, *Proc. Natl. Acad. Sci. USA* **2018**, *115*, E1374.
- [46] D. Kang, S. M. Lee, Z. Li, A. Seyedi, J. O'Brien, J. Xiao, J. Yoon, *Adv. Opt. Mater.* **2014**, *2*, 373.
- [47] J. P. Turpin, J. A. Bossard, K. L. Morgan, D. H. Werner, P. L. Werner, *Int. J. Antennas Propag.* **2014**, *2014*, 429837.
- [48] J.-Y. Ou, E. Plum, L. Jiang, N. I. Zheludev, *Nano Lett.* **2011**, *11*, 2142.
- [49] O. Böstman, H. Pihlajamäki, *Biomaterials* **2000**, *21*, 2615.
- [50] S. W. Hwang, H. Tao, D. H. Kim, H. Cheng, J. K. Song, E. Rill, M. A. Brenckle, B. Panilaitis, S. M. Won, Y. S. Kim, Y. M. Song, K. J. Yu, A. Ameen, R. Li, Y. Su, M. Yang, D. L. Kaplan, M. R. Zakin, M. J. Slepian, Y. Huang, F. G. Omenetto, J. A. Rogers, *Science* **2012**, *337*, 1640.
- [51] *Handbook of Optical Constants of Solids* (Ed: E. D. Palik), Academic Press, New York, NY, USA **1985**.
- [52] S. Larouche, L. Martinu, *Appl. Opt.* **2008**, *47*, C219.
- [53] R. Hu, X. Luo, S. Liu, *IEEE Photonics Technol. Lett.* **2011**, *23*, 1673.
- [54] S.-K. Kang, G. Park, K. Kim, S.-W. Hwang, H. Cheng, J. Shin, S. Chung, M. Kim, L. Yin, J. C. Lee, K.-M. Lee, J. A. Rogers, *ACS Appl. Mater. Interfaces* **2015**, *7*, 9297.

ADVANCED OPTICAL MATERIALS

Supporting Information

for *Advanced Optical Materials*, DOI: 10.1002/adom.201800146

High Performance, Biocompatible Dielectric Thin-Film
Optical Filters Integrated with Flexible Substrates and
Microscale Optoelectronic Devices

*Changbo Liu, Qianyi Zhang, Dan Wang, Guanlei Zhao, Xue
Cai, Lizhu Li, He Ding, Kaiyuan Zhang, Huachun Wang,
Deying Kong, Lan Yin, Lei Liu, Guisheng Zou, Lingyun Zhao,
and Xing Sheng**

Supporting Information

High Performance, Biocompatible Dielectric Thin-Film Optical Filters Integrated with Flexible Substrates and Microscale Optoelectronic Devices

*Changbo Liu, Qianyi Zhang, Dan Wang, Guanlei Zhao, Xue Cai, Lizhu Li, He Ding, Kaiyuan Zhang, Huachun Wang, Deying Kong, Lan Yin, Lei Liu, Guisheng Zou, Lingyun Zhao and Xing Sheng**

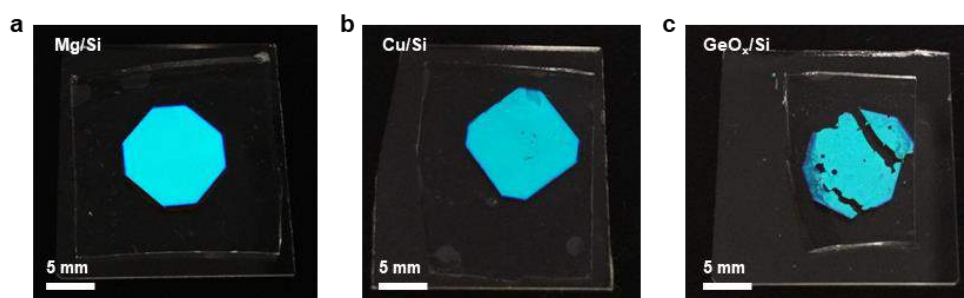
Experimental results of released flexible filters

Figure S1. Photographs of flexible filter membranes released from different sacrificial layers on Si substrates. a) Mg as sacrificial layer, b) Cu as sacrificial layer, c) GeO_x as sacrificial layer.

Optical simulation

Simulation results for light transmission of thin-film filters and EQE of PV detectors with and without filters are calculated based on transfer matrix method, details of which are provided here.

First define the propagation direction, which is illustrated in **Figure S2**. When wave propagates along the x axis from left to right, the expression of the electric field is

$$E_{1+} = |E_{1+}| \exp[-ik_1x]; \tag{S1}$$

when wave propagates in the opposite direction, it becomes

$$E_{1-} = |E_{1-}| \exp[ik_1x], \tag{S2}$$

and

$$k_1 = \frac{2\pi}{\lambda} n_1. \tag{S3}$$

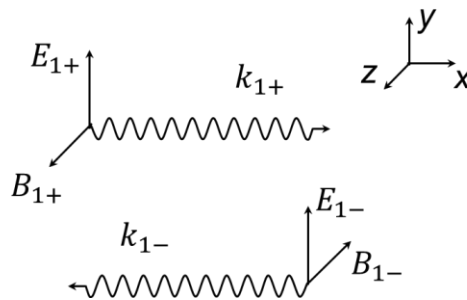


Figure S2. Defining the positive direction of propagation.

Thin-film filters consist of boundaries between different homogenous media, as shown in

Figure S3. The boundary conditions are

$$\begin{aligned} E_1^{\parallel} &= E_2^{\parallel} \\ B_1^{\parallel} &= B_2^{\parallel} \end{aligned} \quad (\text{S4})$$

From Maxwell Equations, it becomes

$$\begin{aligned} E_{1+} &= \frac{1}{2} \left(1 + \frac{n_2}{n_1} \right) E_{2+} + \frac{1}{2} \left(1 - \frac{n_2}{n_1} \right) E_{2-} \\ E_{1-} &= \frac{1}{2} \left(1 - \frac{n_2}{n_1} \right) E_{2+} + \frac{1}{2} \left(1 + \frac{n_2}{n_1} \right) E_{2-} \end{aligned}, \quad (\text{S5})$$

which can be written in matrix form:

$$\begin{bmatrix} E_{1+} \\ E_{1-} \end{bmatrix} = \begin{bmatrix} \frac{1}{2} \left(1 + \frac{n_2}{n_1} \right) & \frac{1}{2} \left(1 - \frac{n_2}{n_1} \right) \\ \frac{1}{2} \left(1 - \frac{n_2}{n_1} \right) & \frac{1}{2} \left(1 + \frac{n_2}{n_1} \right) \end{bmatrix} \begin{bmatrix} E_{2+} \\ E_{2-} \end{bmatrix} = D_{12} \begin{bmatrix} E_{2+} \\ E_{2-} \end{bmatrix}. \quad (\text{S6})$$

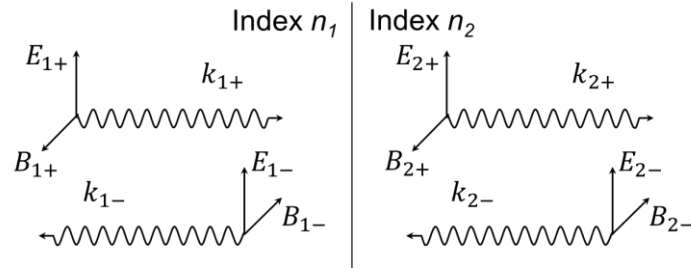


Figure S3. Plane wave incident on a single surface.

Propagation in homogenous medium has the relations (**Figure S4**)

$$\begin{aligned} E'_{2+} &= |E_{2+}| \exp[-ik_2(x+d_2)] = E_{2+} \exp[-ik_2d_2] = E_{2+} \exp\left[-i\frac{2\pi}{\lambda}n_2d_2\right] \\ E'_{2-} &= |E_{2-}| \exp[ik_2(x+d_2)] = E_{2-} \exp[ik_2d_2] = E_{2-} \exp\left[i\frac{2\pi}{\lambda}n_2d_2\right] \end{aligned}, \quad (\text{S7})$$

and

$$\begin{bmatrix} E'_{2+} \\ E'_{2-} \end{bmatrix} = \begin{bmatrix} \exp\left[i\frac{2\pi}{\lambda}n_2d_2\right] & 0 \\ 0 & \exp\left[-i\frac{2\pi}{\lambda}n_2d_2\right] \end{bmatrix} \begin{bmatrix} E_{2+} \\ E_{2-} \end{bmatrix} = P_2 \begin{bmatrix} E_{2+} \\ E_{2-} \end{bmatrix}. \quad (\text{S8})$$

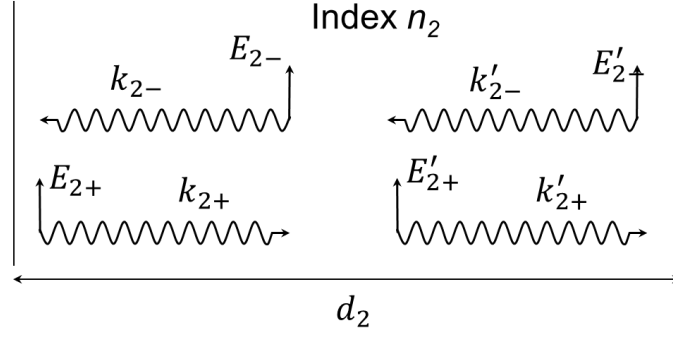


Figure S4. Plain wave propagating in homogeneous medium.

Figure S5 shows model geometry of light traveling through a number of layers. The following matrix relation can be deduced referring to Equation S6 and S8:

$$\begin{bmatrix} E_{1+} \\ E_{1-} \end{bmatrix} = D_{12} \begin{bmatrix} E_{2+} \\ E_{2-} \end{bmatrix} = D_{12} P_2 \begin{bmatrix} E'_{2+} \\ E'_{2-} \end{bmatrix} = D_{12} P_2 D_{23} \begin{bmatrix} E_{3+} \\ E_{3-} \end{bmatrix} = D_{12} P_2 D_{23} P_3 \dots P_{N-1} D_{(N-1)N} \begin{bmatrix} E_{N+} \\ E_{N-} \end{bmatrix} = \begin{bmatrix} M_{11} & M_{12} \\ M_{21} & M_{22} \end{bmatrix} \begin{bmatrix} E_{N+} \\ E_{N-} \end{bmatrix} \quad (\text{S9})$$

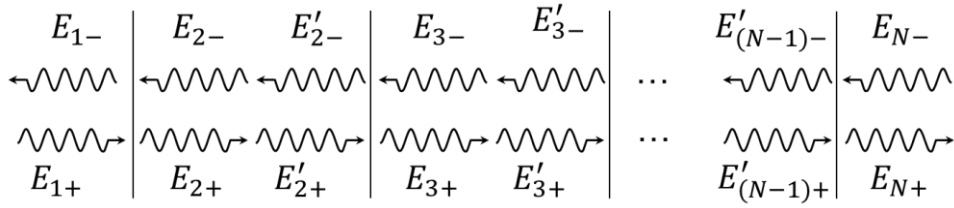


Figure S5. Plain wave traveling through a number of layers.

and

$$E_{N-} = 0. \quad (\text{S10})$$

The irradiance can be calculated

$$\mathbf{I} = \frac{1}{2} \text{Re}(\mathbf{E} \times \mathbf{H}^*) = \text{Re} \left(\frac{1}{2} \mathbf{y} \mathbf{E} \mathbf{E}^* \hat{s} \right) = \frac{1}{2} n \gamma \mathbf{E} \mathbf{E}^* \hat{s} \quad (\text{S11})$$

or

$$I \propto n \times |E|^2. \quad (\text{S12})$$

Reflectance R is defined as the ratio of the reflected and incident irradiances and transmittance T as the ratio of the transmitted and incident irradiances:

$$R = \frac{I_r}{I_i} = \left| \frac{E_{1-}}{E_{1+}} \right|^2 = \left| \frac{M_{21}}{M_{11}} \right|^2 \quad (\text{S13})$$

$$T = \frac{I_t}{I_i} = \frac{n_N}{n_1} \left| \frac{E_{N+}}{E_{1+}} \right|^2 = \frac{n_N}{n_1} \left| \frac{1}{M_{11}} \right|^2. \quad (\text{S14})$$

For absorptive material, include

$$\tilde{n} = n - ik. \quad (\text{S15})$$

For oblique angles, boundary conditions are

$$\begin{aligned} \varepsilon_1 E_1^\perp &= \varepsilon_2 E_2^\perp \\ E_1^\parallel &= E_2^\parallel \\ B_1^\perp &= B_2^\perp, \\ \frac{1}{\mu_1} B_1^\parallel &= \frac{1}{\mu_2} B_2^\parallel \end{aligned} \quad (\text{S16})$$

and from Snell's law,

$$n_1 \sin \theta_1 = n_2 \sin \theta_2. \quad (\text{S17})$$

S-polarised light, in the notation of **Figure S6**, is

$$\begin{bmatrix} 1 & 1 \\ \frac{n_1}{\mu_1} \cos \theta_1 & -\frac{n_1}{\mu_1} \cos \theta_1 \end{bmatrix} \begin{bmatrix} E_{1+} \\ E_{1-} \end{bmatrix} = \begin{bmatrix} 1 & 1 \\ \frac{n_2}{\mu_2} \cos \theta_2 & -\frac{n_2}{\mu_2} \cos \theta_2 \end{bmatrix} \begin{bmatrix} E_{2+} \\ E_{2-} \end{bmatrix}, \quad (\text{S18})$$

and p-polarised light can be described as

$$\begin{bmatrix} \cos \theta_1 & \cos \theta_1 \\ \frac{n_1}{\mu_1} & -\frac{n_1}{\mu_1} \end{bmatrix} \begin{bmatrix} E_{1+} \\ E_{1-} \end{bmatrix} = \begin{bmatrix} \cos \theta_2 & \cos \theta_2 \\ \frac{n_2}{\mu_2} & -\frac{n_2}{\mu_2} \end{bmatrix} \begin{bmatrix} E_{2+} \\ E_{2-} \end{bmatrix}. \quad (\text{S19})$$

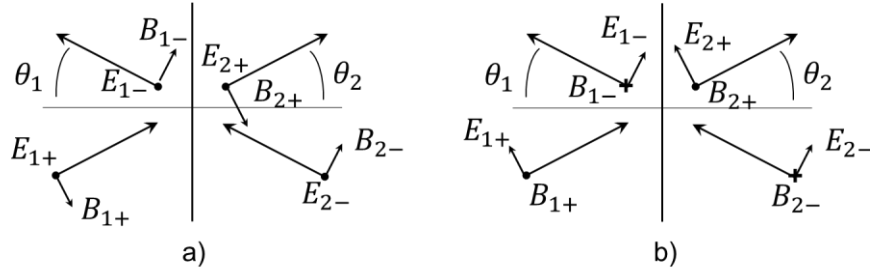


Figure S6. a) Convention defining the positive directions of electric and magnetic vectors for s-polarised light (TE waves). b) Convention defining the positive directions of electric and magnetic vectors for p-polarised light (TM waves).

Light of oblique incidence propagating in homogeneous medium (**Figure S7**) are analogous to that of normal incidence:

$$\begin{bmatrix} E_{2+} \\ E_{2-} \end{bmatrix} = \begin{bmatrix} \exp\left[i\frac{2\pi}{\lambda}n_2d_2\cos\theta_2\right] & 0 \\ 0 & \exp\left[-i\frac{2\pi}{\lambda}n_2d_2\cos\theta_2\right] \end{bmatrix} \begin{bmatrix} E'_{2+} \\ E'_{2-} \end{bmatrix}. \quad (\text{S20})$$

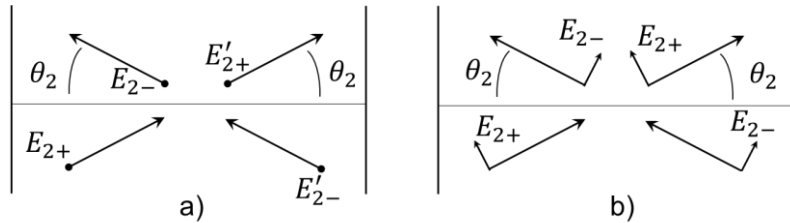


Figure S7. a) S-polarised light and b) p-polarised light propagating in homogeneous medium with oblique angles.

The LED emission profile is modeled by Monte Carlo based ray tracing methods (TracePro free trial version). A file source with 200,000 rays, which emits light with the wavelength of 470 nm towards all directions obeying Lambert’s cosine law, is traced to get the polar candela distribution plot. It works as multiple quantum wells, emitting light towards two opposite directions from a plane in the middle of the LED.

The solid model is combined with a filter and a LED. The filter functions by setting surface property of the underside of the LED, and reflects most of the emitted light. The LED size is 140 μm by 190 μm by 7 μm , and the refractive index of the LED is set to 2.39, which is the average refractive index of ordinary and extraordinary rays in GaN when the wavelength of light is 470 nm.